Temperature Control Strategies of Atmospheric Plasma Jet for Tissue Treatment

Bingkai Wang, Xu Yan, and Zilan Xiong

***Abstract*—Besides the charged particles and neutral reactive species, the temperature effect is another significant issue needs to concern during the plasma treatment of biological tissue, which has effects on therapeutic efficacy and the risk of burns. Due to the influence of multiple factors on the temperature effect, it's a complex nonlinear problem. In this study, temperature rise and distribution uniformity under different parameters and moving trajectories on porcine skin were investigated, and then a surface temperature control strategy was proposed. A 3-D electric motor control platform was constructed for the jet moving during the treatment. First, the effects of factors, such as distance, voltage, and flow rate on temperature variation over porcine skin surface, were analyzed, and the trends of temperature variation under single-factor influence were summarized. Then, the temperature distribution of fixed-point treatment and the temperature superposition effect on the tissue surface under different trajectories were explored, and a trajectory scheme for achieving homogeneous temperature distribution was proposed. Finally, a closed-loop control model was designed to achieve the control objectives of constant temperature holding over a certain surface area and resistance to high-temperature interference in real time. This control scheme also has reference significance for other surface treatments such as material processing.**

***Index Terms*—Biological tissues, plasma jet, temperature control, temperature superposition effect, temperature variation patterns.**

I. Introduction

IN RECENT years, atmospheric pressure plasma jet (APPJ), as a novel plasma source, has attracted increasing attention and research. With advantages, such as low invasiveness, rapidity, and high efficiency, plasma jet has broad prospects for applications in the field of biomedical sciences, such as skin disease treatment, promoting wound healing, blood coagulation, and tumor reduction [1], [2], [3], [4], [5], [6]. Meanwhile, due to its ability to locally generate thermal, chemical, and electrical effects and transfer them to the treated materials, APPJ has been widely employed in material processing, such as polymerization, etching, and surface activation [7], [8], [9]. It also plays a significant role in environmental protection [10].

As an emerging medical device, plasma jet equipment has been rapidly developed. There have been an increasing number of atmospheric pressure plasma devices approved for clinical use both domestically and internationally, such as kINPen [11] and SteriPlas [12]. Existing research primarily focuses on the plasma source and its physicochemical effects on biological tissues. The investigation of plasma jet sources includes their simulation, diagnostics, and various improvements. Numerical simulations are employed to explore the development process of plasma jet [13], [14], while electrical and optical signals are used to diagnose the density and distribution characteristics of electrons, ions, radicals, and molecules in the plasma [15]. Various improvements to the plasma source involve utilizing different driving power sources, carrier gases, and discharge structures to achieve specific medical applications in different scenarios [16], [17], [18]. Regarding the physicochemical effects on biological tissues, this encompasses the transport of various active species in gas and liquid phases, as well as chemical reaction processes [19], [20], and their medical applications such as sterilization and wound healing promotion.

During the plasma jet treatment of biomedical tissues in practice, the temperature rise and distribution should also be considered. However, existing studies have focused on the electrical, optical [21], and chemical perspectives of the plasma jet, there has been a limited emphasis on its temperature characteristics when treatment of biomedical tissues [22], [23]. On the one hand, temperature directly influences the chemical reactions, and an appropriate reaction temperature can enhance the treatment efficacy of plasma jets [24], [25]. On the other hand, due to the high energy and temperature characteristics of ions and electrons in plasma jets, long-time exposure of biological tissues to elevated temperatures can lead to severe consequences such as local thermal burns [26], [27]. Therefore, temperature regulation during the treatment of biological tissues with plasma jets is a crucial matter.

Currently, regarding the issue of temperature control in the application of plasma jet, there are numerous challenges and difficulties due to the direct relationship between temperature variations and factors, such as flow rate, distance, voltage, and gas. This complex nonlinear system presents ongoing research

Manuscript received 11 September 2023; revised 1 November 2023 and 29 November 2023; accepted 30 November 2023. Date of publication 7 December 2023; date of current version 3 January 2024. This work was supported in part by the National Natural Science Foundation of China under Grant 51907076 and Grant 52077006, and in part by the Beijing Natural Science Foundation under Grant 7232332. *(Corresponding author: Zilan Xiong.)*

This work did not involve human subjects or animals in its research.

Bingkai Wang and Zilan Xiong are with the State Key Laboratory of Advanced Electromagnetic Engineering and Technology, Huazhong University of Science and Technology, Wuhan 430074, Hubei, China (e-mail: zilanxiong@hust.edu.cn).

Xu Yan is with the Department of Pathophysiology, Beijing Neurosurgical Institute/Beijing Tiantan Hospital, Capital Medical University, Beijing 100070, China.

Color versions of one or more figures in this article are available at https://doi.org/10.1109/TRPMS.2023.3340154.

Digital Object Identifier 10.1109/TRPMS.2023.3340154

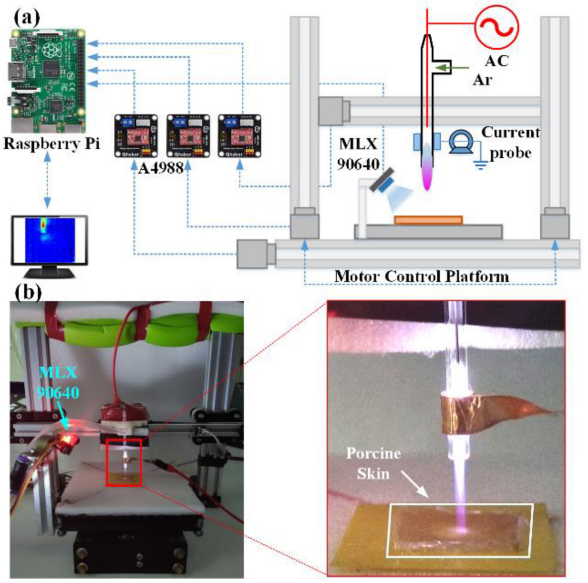

Fig. 1. (a) Experimental platform for temperature control. (b) Biological tissue treated by plasma jet.

challenges. In existing research on surface temperature control for APPJs, infrared camera or spectrometers have been used to collect thermal data from the object surface, and parameters, such as voltage, flow rate, and distance, have been adjusted to achieve control of the maximum surface temperature or thermal dose under plasma jet treatment [28], [29], [30], [31]. However, the above literature does not involve real-time adjustment of the overall surface temperature and temperature distribution of the object, which can directly and quickly characterize and adjust the surface reaction state. Therefore, surface temperature control strategies in the biomedical application of plasma jets, especially the high temperature restrain and homogeneous temperature distribution during treatment, play a significant role in improving the safety and effectiveness of medical treatments.

In view of this, this study investigates surface temperature control strategies of plasma jets for tissue treatment. Plasma jets at different distances, flow rates, and voltages are used to treat biological tissues, and the temporal variations of temperature at the treatment point are explored. Subsequently, by designing the movement trajectory of the plasma jet on the surface of biological tissues, the cumulative effect of temperature on the tissue surface is examined to achieve homogeneous temperature distribution. Finally, control strategies are implemented to achieve constant temperature holding over a certain surface area and resistance against temperature interference.

II. Experimental Platform and Methods

A. Experimental Platform

Fig. 1 shows the experimental platform for temperature control of plasma jet. A needle-ring configuration is employed for the plasma jet, where the high-voltage electrode consists of a steel needle with a diameter of 0.6 mm, connected to a high-voltage ac power supply (CTP-2000K; Corona Lab). The ground electrode is wrapped with a copper foil of width 9.5-mm around the quartz tube. The bottom end of the quartz tube is positioned 5 mm away from the nozzle, and the upper end is situated 5 mm away from the needle electrode. The inner diameter of the quartz tube is 3 mm, while the outer diameter is 5 mm. Argon gas is used as the carrier gas. The porcine skin is used in this study as the biological tissue, which exhibits similar characteristics to human tissue despite its lower temperature of approximately 24 °C compared to the normal human body temperature of about 35 °C. Hence, it serves as an appropriate model for human tissue. The size of the porcine skin sample is approximately 30 mm × 25 mm × 5 mm (length × width × height).

In order to achieve precise control of the plasma jet for biological tissues treatment, an electric motor control platform was constructed. This platform adopts the Cartesian coordinate system, where the x, y, and z axes are driven by four stepper motors (two motors for the z-axis) with a speed of 4.8 mm/s. It enables accurate moving in all three directions (± 1 mm) of XYZ. The plasma jet is fixed on the x-axis and can follow the motor movement in the XZ direction. The plate for placing biological tissues is fixed on the y-axis, and the movement of the plate in the forward and backward directions is controlled by the stepper motor on the y-axis, thereby achieving movement in the Y-direction. The stepper motors are driven by A4988 stepper motor driver boards, controlled by a Raspberry Pi via GPIO. The surface temperature measurement module adopts an MLX90640 infrared thermal sensor, which can accurately measure the surface temperature of the target object in a specific area and temperature range at close range. It is connected to the Raspberry Pi's I2C interface, and the temperature data is read through Python code and displayed in real time on the monitor as a thermal image. The temperature measurement module MLX90640 is fixed to the lower left corner of the plate using a bracket and measures the surface temperature of the biological tissue located at the center of the plate from above. The relative positions of the temperature measurement module and the biological tissue remain fixed, ensuring that the area of the biological tissue in the thermal image remains constant.

Furthermore, in order to analyze the temperature distribution on the surface of biological tissue, an infrared camera (D384A; Guide Infrared) is utilized to capture infrared images, which were subsequently imported into the ThermoTools software for analysis in detail. It should be noted that both the MLX90640 temperature sensor module and the infrared camera are used to measure the surface temperature of biological tissue. The MLX90640 temperature sensor is chosen for its small size, convenience of use, easy installation on a motor platform, and compatibility with small embedded devices for temperature measurement and control in time. The infrared camera is utilized for a more intuitive and accurate observation of the overlaying effect of surface temperatures in biological tissues, combined with professional software to analyze the temperature characteristics in specific regions of the biological tissue. All results related to the temperature heat maps mentioned in this article are obtained through analysis using the infrared camera, while temperature variation over time and regulation of surface temperature are acquired by the MLX90640 temperature sensor module.

TABLE I
EXPERIMENTAL PARAMETERS

Vpp\Flow	0.6SLM	0.5SLM	0.4SLM
9kV	1.5cm	1.5cm	1.5cm
	2cm	2cm	2cm
	2.5cm	2.5cm	2.5cm
8kV	1.5cm	1.5cm	1.5cm
	2cm	2cm	2cm
	2.5cm	2.5cm	2.5cm
7kV	1.5cm	1.5cm	1.5cm
	2cm	2cm	2cm
	2.5cm	2.5cm	2.5cm

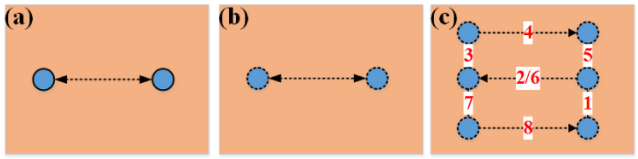

Fig. 2. Plasma jet operating trajectories. (a) Trajectory 1. (b) Trajectory 2. (c) Trajectory 3.

B. Temperature Variation Measurement at Fixed Treatment Point

In the process of plasma jet treatment of biological tissues, there are several factors that influence the surface temperature, including distance, voltage, flow rate, angle, and time. Considering the feasibility of comprehensive regulation, distance, voltage, and flow rate were selected as the variables for exploration. The experimental parameters designed for this study are presented in Table I, encompassing a total of 27 different combinations of distance, voltage, and flow rate conditions. Here, the voltage is represented by the peak-to-peak value (Vpp) at a frequency of 8 kHz.

The plasma jet is positioned directly above the center of the plate, which coincides with the center of the biological tissue. By adjusting the z-axis motor, the distance is varied while maintaining a fixed position in the XY-plane. The temperature values on the surface of the porcine skin are collected using the temperature measurement module. The treated time of each condition is set at 180 s, with temperature data recorded every 10 s.

C. Temperature Superposition Test

In practical applications, to achieve homogeneous treatment over the whole treatment area, the plasma jet needs to move back and forth under a certain trajectory, simultaneously heating and dissipating heat within different positions. This process is not a linear accumulation. Therefore, to obtain homogeneous temperature distribution over the treatment area, it is worth exploring the temperature superposition effect under different moving trajectories. Fig. 2 illustrates three movement trajectories for testing under fixed distance, voltage, and flow rate conditions.

1) *Trajectory 1:* Treat the biological tissue at the left point for 10 s, then move at a constant speed to the right point for 10 s. Repeat this process between the two points, with a total treatment time of 180 s.
2) *Trajectory 2:* Perform a back-and-forth movement at a constant speed between the left and right points without stopping at either point. The total treatment time is 180 s.
3) *Trajectory 3:* Move back and forth in the following trajectory on the biological tissue: 1-2-3-4-5-6-7-8. Do not stop at any point. The total treatment time is 180 s.

III. RESULTS AND DISCUSSION

A. Temperature Distribution and Variation Results at Fixed Treatment Point

The typical voltage and current waveforms under 8 kV, 0.5-SLM flow rate, and 1.5-cm distance are shown in Fig. 3(a). The voltage is a standard sinusoidal wave with a Vpp of 8 kV and the frequency is fixed at 8 kHz. The current fluctuates near the junction of positive and negative voltage values. Fig. 3(b) illustrates the typical temperature distribution on the surface of the biological tissue at a fixed treatment point. A high-temperature region is formed around the plasma jet processing point, with the center serving as the focal point. As the distance from the center point increases, the temperature gradually decreases. The untreated areas show no significant temperature increase. The temperature distribution along the line L exhibits a distinct unimodal shape, with a difference of approximately 3.8 °C between the highest and lowest temperature values. The average temperature of the entire region R is 28.6 °C, with a variance of 0.78, indicating an uneven temperature distribution.

According to the experimental conditions in Table I, temperature data within 180 s were collected for each condition. The maximum temperature value in biological tissue was selected, and the trend of temperature change over time was plotted. Since the data trends and distributions are basically consistent, representative data were selected for illustration in Fig. 4 when conducting a comparative analysis of single variables. The following sections analyze the effects of distance, voltage, and flow rate on temperature variation separately.

1) The temperature–time curves under different distances with the same voltage and flow rate are shown in Fig. 4(a). It can be observed that the temperature increases with the treatment time, and as the distance increases, the temperature rise under the same conditions gradually decreases. At the distance of 1.5 cm, the temperature rise reaches 5.5 °C, which corresponds to a surface temperature of 41 °C on the human skin. However, at distances of 2.0 and 2.5 cm, the temperature rise is only around 1 °C–2 °C and shows a saturated trend, indicating an insignificant temperature elevation effect. By increasing the distance, the surface temperature of the biological tissue can be rapidly reduced.
2) The temperature–time curves under different voltages with the same flow rate and distance are shown in Fig. 4(b). As the voltage increases, the temperature rise under the same conditions gradually increases. The plasma discharge region acts as the heat source, and with higher voltage, there is a corresponding increase in heat generation, resulting in a more pronounced heating effect on the porcine skin. Additionally, a lower voltage leads to an earlier appearance of the saturation trend.

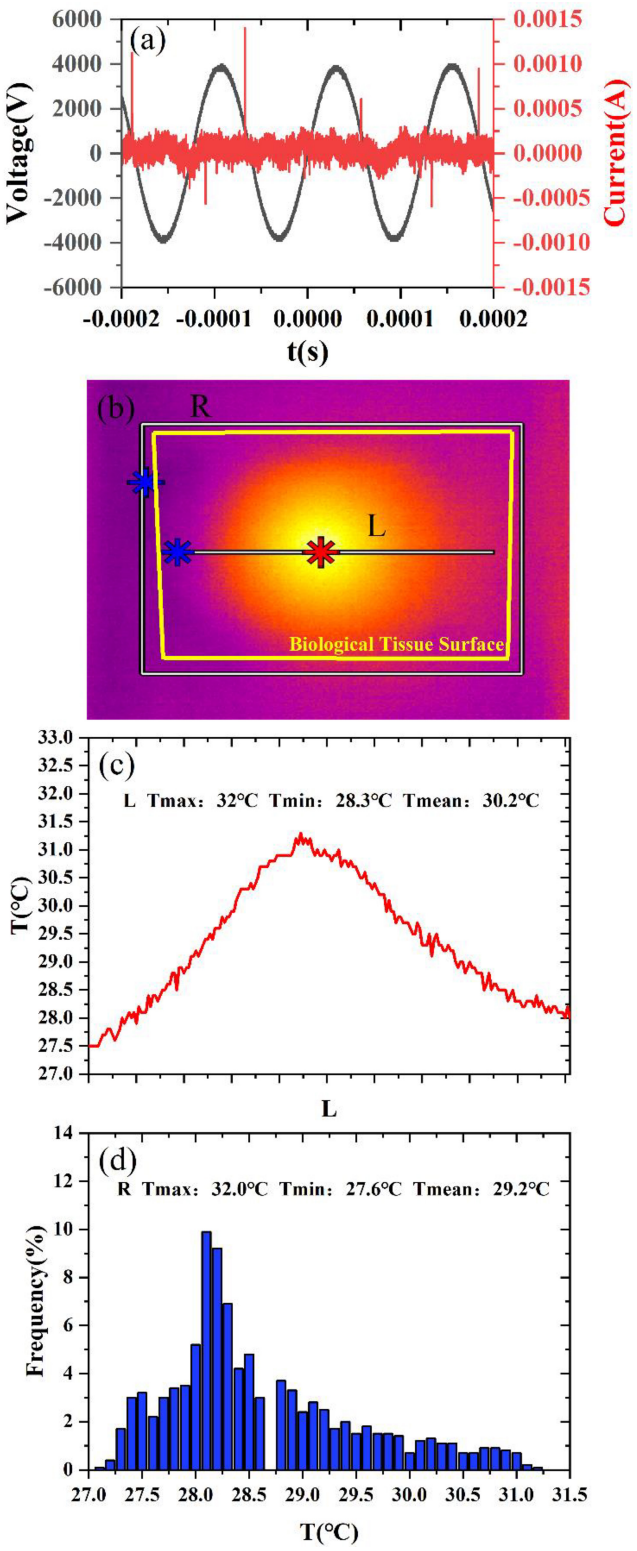

Fig. 3. Typical temperature distribution result at fixed treatment point under 8-kV voltage amplitude, 0.5-SLM flow rate, and 1.5-cm distance. (a) U–I waveform. (b)Temperature heat map (recorded by infrared camera). (c) Temperature curve of line L. (d) Temperature histogram of area R.

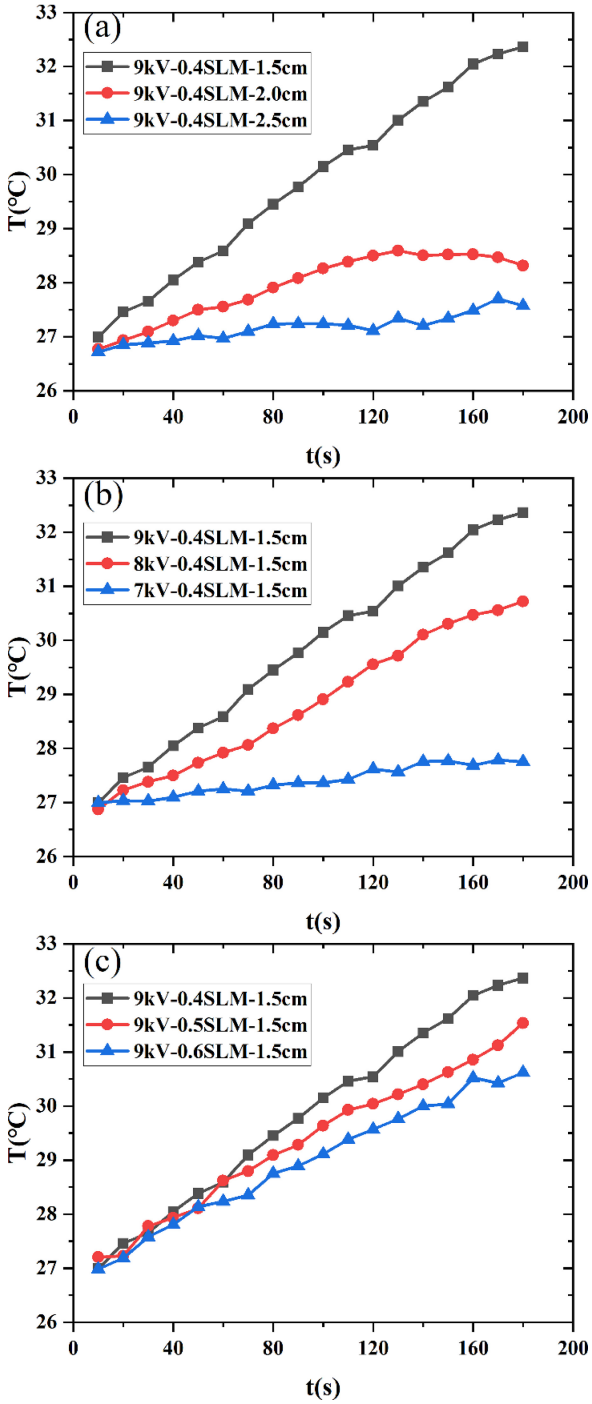

Fig. 4. Temperature variation over time. (a) Different distances with the same voltage and flow rate. (b) Different voltages with the same flow rate and distance. (c) Different flow rates with the same voltage and distance.

At 7 kV, the temperature rise is only 0.5 °C, while at 8 kV, the saturation trend begins around 150 s. However, at 9 kV, there is still an upward trend in temperature.

3) The temperature–time curves under different flow rates with the same voltage and distance are shown in Fig. 4(c). As the flow rate increases, the temperature rise under the same conditions gradually decreases. This is because the airflow affects convective heat dissipation, and with a larger flow rate, heat diffusion occurs more quickly, resulting in a lower temperature rise. Additionally, the flow rate gradients used here are 0.4, 0.5, and 0.6 SLM, which have a small difference. Within the range of 0–50 s, the temperature levels of the three flow rates are basically the same. However, as time goes on, differences in the temperature rise effects can still be observed.

The following conclusions can be drawn from the analysis of temperature variation curves: under the aforementioned voltage, flow rate, and distance conditions, the temperature change on the porcine surface treated by plasma jet within 180 s is positively correlated with voltage, while negatively correlated with gas flow rate and distance. As the voltage level decreases, the increase in gas flow rate and distance, the saturation trend presented by the temperature rise curve becomes increasingly apparent.

B. Temperature Superposition Results

As demonstrated above, the temperature distribution over a certain surface area at a fixed treatment point is uneven. In order to obtain homogeneous temperature distribution, the porcine skin was treated using three different moving trajectories (as shown in Fig. 2) under the conditions of 8-kV voltage amplitude, 0.5-SLM flow rate, and 1.5-cm distance. After each treatment, the temperature distribution on the porcine skin surface was rapidly recorded using an infrared camera. The results of the temperature analysis for the biological tissue area are as follows.

1) Trajectory 1: As shown in Fig. 5, after treating the porcine skin with plasma jet along trajectory 1, two thermal centers appeared at two points on the porcine skin surface. By extracting the temperature distribution along straight line L1, a double-peak structure can be observed. The highest temperatures at the two thermal centers were 30.5 °C and 29.8 °C, respectively. In the region along the line between the two thermal centers, there were peaks and valleys of temperature due to the shorter heating time. The temperature difference between the highest and lowest temperatures values along line L1 is 2.2, which is much smaller than the temperature difference observed under fixed-point treatment. To analyze the overall temperature distribution, a temperature histogram of the biological tissue area R1 was plotted, and the proportions of different temperatures were calculated. The temperature ranged from 26.9 °C to 30.6 °C, with a concentrated distribution around 28.2 °C. The obtained variance was 0.62, indicating a better level of temperature uniformity throughout the region than area R under fixed-point treatment processing.

2) Trajectory 2: As shown in Fig. 6, after treating the porcine skin with a plasma jet along trajectory 1, a thermal center region appeared along the trajectory. During the repetitive operation of the plasma jet, the heating effect on the porcine skin surface along the trajectory was evident. The temperature distribution along straight line L2 exhibited a parabolic shape, with a temperature difference between the highest and lowest points reaching 3.2 °C. Regarding the overall temperature distribution of the biological tissue, the temperature histogram of area R2 revealed a range of temperature variation from 26.9 °C to 30.6 °C, which was larger than the temperature range observed for trajectory 1. The obtained variance for this region was 1.16, indicating a relatively uneven temperature distribution throughout the area. Compared with the situation under fixed-point treatment, the temperature distribution shape and temperature difference

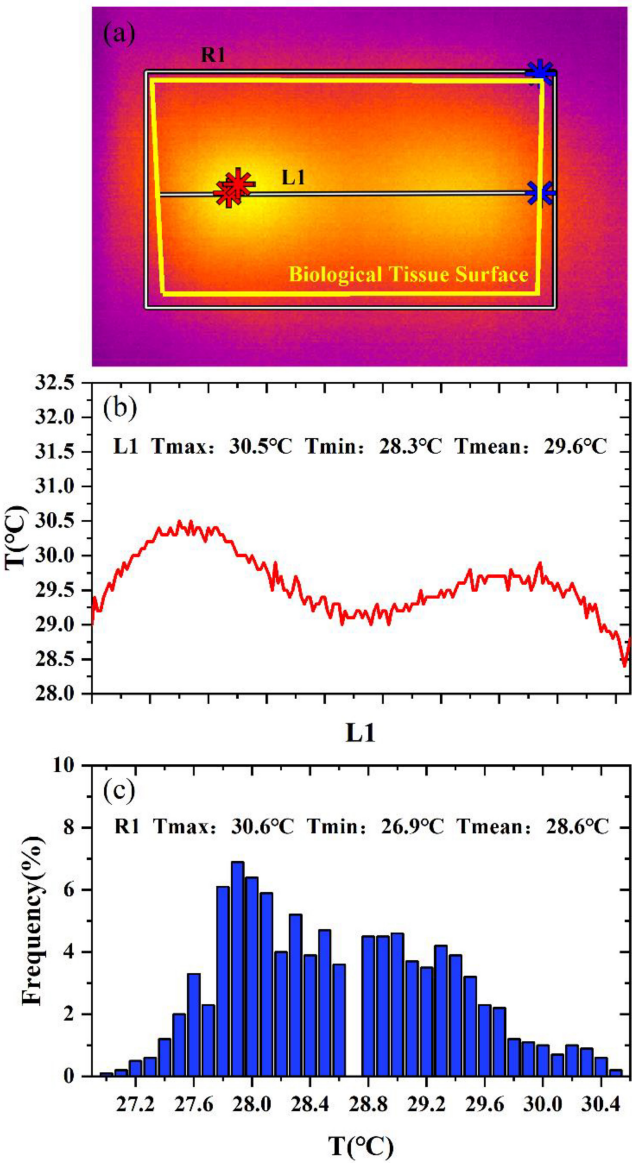

Fig. 5. Temperature distribution result for trajectory 1. (a) Temperature heat map. (b) Temperature curve of line L1. (c) Temperature histogram of area R1.

along lines L and L2 exhibit similar patterns. The temperature difference along L2 is slightly smaller. The temperature variance in region R2 is larger than that in region R. This is because during the movement process, heating is concentrated along the lines rather than at the processing points, leading to a larger temperature difference range relative to the entire region. However, the temperature values in the connected region above an average temperature of 30.6 °C were relatively uniform, which also provides inspiration for the design of Trajectory 3.

3) Trajectory 3: Inspired by the relatively uniform temperature distribution along the trajectory in Trajectory 2, a moving path for Trajectory 3 was designed as shown in Fig. 7. Trajectory 3 traveled the entire porcine skin surface, resulting in a relatively uniform overall temperature distribution. Along the same line L3 as Trajectories 1 and 2, the temperature distribution exhibited a parabolic shape. However, the temperature variation range was 28.9 °C–29.9 °C, with a temperature

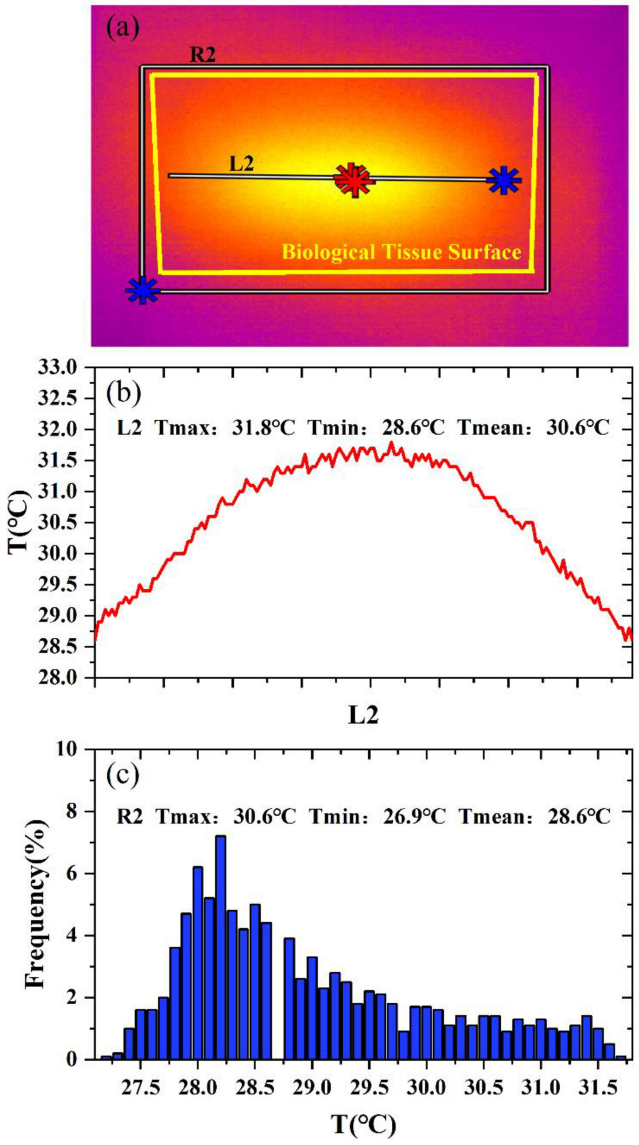

Fig. 6. Temperature distribution result for trajectory 2. (a) Temperature heat map. (b) Temperature curve of line L2. (c) Temperature histogram of area R2.

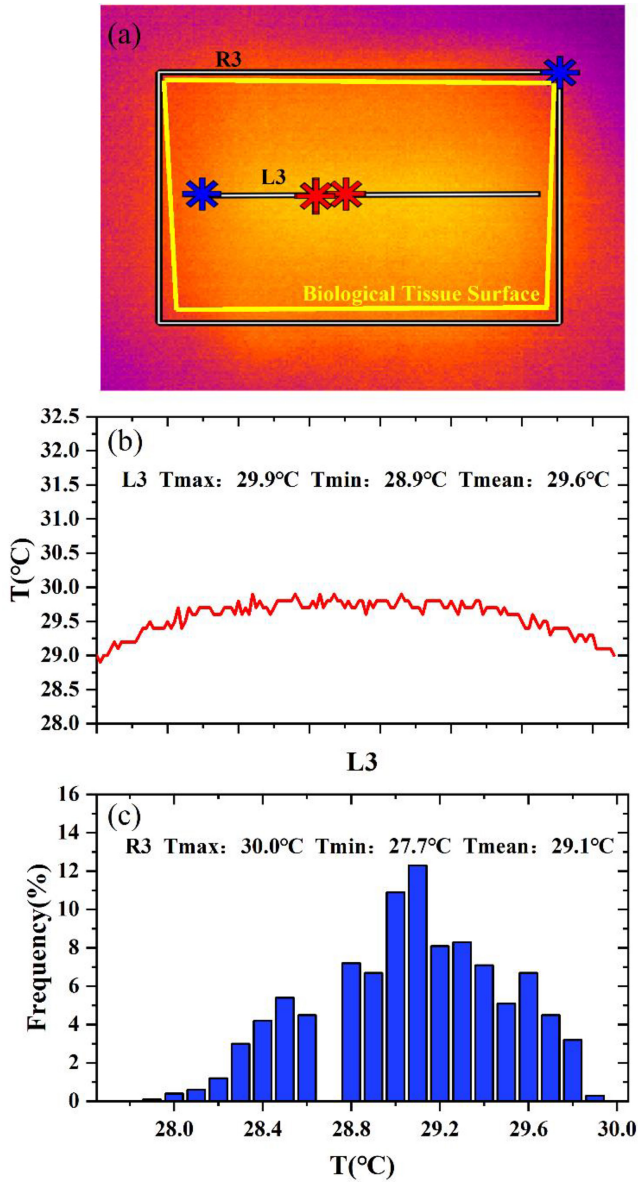

Fig. 7. Temperature distribution result for trajectory 3. (a) Temperature heat map. (b) Temperature curve of line L3. (c) Temperature histogram of area R3.

difference of only 1 °C, much smaller than those of fixed-point treatment, Trajectories 1 and 2. In the temperature histogram of the overall porcine skin surface, the temperature range was 27.7 °C–30.0 °C, with a concentration around the mean value of 29.1 °C. The obtained variance for this region was 0.17, indicating a very good level of uniformity.

Based on the analysis of temperature superposition under different moving trajectories, it can be observed that due to the presence of the gas flow field, heating and cooling occur simultaneously at different locations. The temperature superposition is nonlinear. The surface temperature distribution under the fixed treatment point exhibits a pattern where the temperature is higher at the processing point and lower in the surrounding areas, and the uniformity of the temperature distribution is relatively poor. After the attempts and summarization of different trajectories, Trajectory 3 was found to achieve a relatively homogeneous temperature distribution, which lays the foundation for subsequent temperature control.

C. Real-Time Temperature Control Results

Although Trajectory 3 can achieve a uniform temperature distribution, however, in practical applications, achieving optimal treatment results can be accomplished through appropriate temperature settings. Therefore, it is crucial to ensure both temperature uniformity and the ability to adjust the desired temperature value. Based on the investigation results of temperature variations and superposition, a control scheme shown in Fig. 8 is designed. In this scheme, a PID closed-loop control approach was employed to regulate the temperature of the biological tissue region. The control objective was to minimize the error between the desired temperature target and the temperature of the biological tissue measured by MLX90640. After PID processing, the control output was generated, which corresponds to the distance between the plasma jet and the porcine skin surface along the z-axis height. It was essential to ensure that the temperature in this region

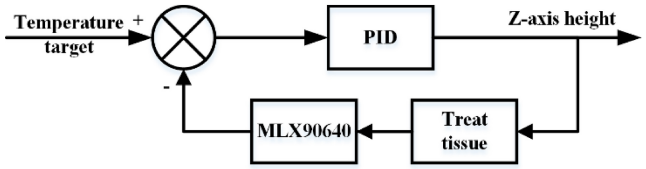

Fig. 8. Temperature control scheme.

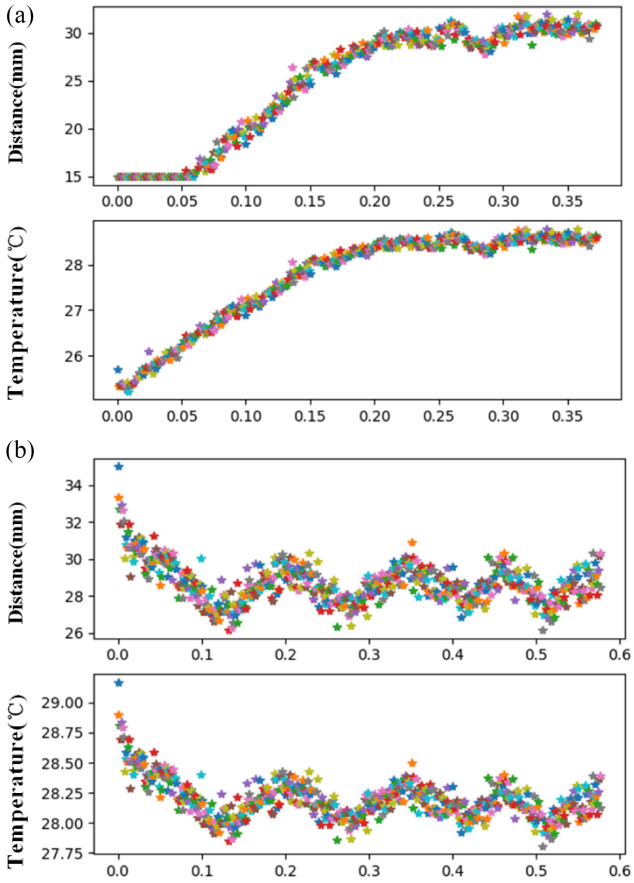

Fig. 9. Real-time temperature and distance variation. (a) Process of increasing the regulated temperature. (b) Process of decreasing the regulated temperature.

remained stable near the target value. Additionally, the system should exhibit a rapid recovery to the target value when subjected to high-temperature disturbances.

Regarding the aspects of achieving constant temperature value and resisting high-temperature disturbances, the experiment was conducted under the conditions of 8-kV voltage and 0.5-SLM flow rate. The *xy*-axis movement followed the trajectory shown in Fig. 2(c). The control objective was to maintain the temperature of the biological tissue region at 28 °C. The parameter values used were $P = 7$, $I = 0.005$, and the distance varied within the range of 15–35 mm. Real-time temperature control was achieved by adjusting the distance in real time.

1) Constant Temperature Holding: As shown in Fig. 9(a) and (b), the real-time variations of distance and temperature during the process of increasing and decreasing the regulated temperature are presented, respectively. It can be observed that the trends of both variables are generally consistent. This is because temperature and distance exhibit a negative correlation, and negative feedback control is employed. In this

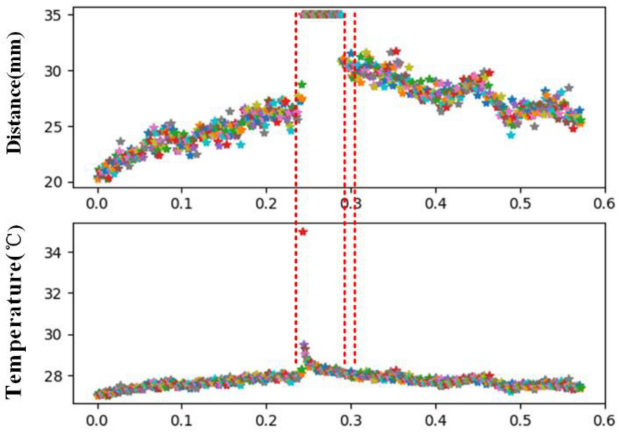

Fig. 10. Temperature and distance variation with under temperature perturbation.

case, the error value and I value are relatively small, with the primary influence coming from the P value. Therefore, the two variables demonstrate a significant positive correlation in their variations. Taking the heating process as an example, initially, when the temperature is below the target value of 28 °C, the distance is adjusted to a closer position, leading to an increase in temperature. When the temperature approaches 28 °C, it starts to fluctuate and gradually stabilizes. The cooling process follows a similar pattern but in the opposite direction.

2) Resistance to High-Temperature Disturbances: As shown in Fig. 10, the real-time variations of distance and temperature under high-temperature disturbances are demonstrated. First, when the temperature of the biological tissue rises to 28 °C, an artificial high-temperature disturbance is introduced, causing the surface temperature of the biological tissue to exceed 35 °C. The distance is rapidly adjusted to the maximum limit of 35 mm to initiate surface tissue cooling. Subsequently, this distance value is maintained until the temperature drops to approximately 28 °C. Once reached, the distance begins to gradually decrease, eventually stabilizing. During this process, both the temperature and the distance experience fluctuations around 28 °C.

IV. Conclusion

Regarding the temperature control issue of plasma jet in biomedical applications, the influence of factors on the surface temperature of biological tissue is analyzed, and the temperature superposition effect is explored through different movement trajectories, finally ultimately achieving temperature control in terms of constant temperature holding over certain surface area and resistance to high-temperature disturbances. The variation of surface temperature during the treatment of porcine skin by plasma jet is positively correlated with voltage, while negatively correlated with gas flow rate and distance. The surface temperature distribution under the fixed treatment point processing exhibits a pattern where the temperature is higher at the processing point and lower in the surrounding areas, and the uniformity of the temperature distribution is relatively poor. The selected movement of plasma jet trajectory on the surface of biological tissue helps achieve a homogeneous surface temperature distribution. The temperature variance in the

region of biological tissue decreased from 0.78 to 0.17, indicating a more favorable distribution of temperature. The designed closed-loop control model and the 3-D electric motor control platform realize the control objectives through moving along the fixed trajectory and adjusting the treatment distance in real time. Temperature control on nonflat surface and different tissues, and the influence of driven power and working gas should be further explored. This approach also provides a reference for plasma jet treatment on other types of materials.

ACKNOWLEDGMENT

All authors declare that they have no known conflicts of interest in terms of competing financial interests or personal relationships that could have an influence or are relevant to the work reported in this article.

REFERENCES

[1] A. Khlyustova, C. Labay, Z. Machala, M. P. Ginebra, and C. Canal, "Important parameters in plasma jets for the production of RONS in liquids for plasma medicine: A brief review," *Front. Chem. Sci. Eng.*, vol. 13, no. 2, pp. 238–252, 2019, doi: 10.1007/s11705-019-1801-8.

[2] S. Bekeschus, S. Iseni, P. Lüttjohann, and K.-D. Weltmann, "Tailored power of an RF plasma jet with admixture of nitrogen or oxygen and its effects on human immune cells," *IEEE Trans. Plasma Sci.*, vol. 49, no. 11, pp. 3336–3343, Nov. 2021, doi: 10.1109/TPS.2021.3087199.

[3] J. Y. Jang et al., "Cold atmospheric plasma (CAP), a novel physicochemical source, induces neural differentiation through cross-talk between the specific RONS cascade and Trk/Ras/ERK signaling pathway," *Biomaterials*, vol. 156, pp. 258–273, Feb. 2018, doi: 10.1016/j.biomaterials.2017.11.045.

[4] Z. Xiong and D. B. Graves, "A novel cupping-assisted plasma treatment for skin disinfection," *J. Phys. D. Appl. Phys.*, vol. 50, no. 5, 2017, Art. no. 5LT01, doi: 10.1088/1361-6463/50/5/05LT01.

[5] Z. Xiong et al., "On the mechanisms of surface microdischarge plasma treatment of onychomycosis: Penetration, uptake, and chemical reactions," *Plasma Process. Polym.*, vol. 18, no. 5, pp. 1–7, 2021, doi: 10.1002/ppap.202000204.

[6] Z. Xiong, J. Roe, T. C. Grammer, and D. B. Graves, "Plasma treatment of onychomycosis," *Plasma Process. Polym.*, vol. 13, no. 6, pp. 588–597, 2016, doi: 10.1002/ppap.201600010.

[7] N. M. Almousa, N. M. Almousa, N. M. Almousa, and M. Bourham, "Simulation of erosion and redeposition of plasma facing materials under transient plasma instabilities," *IEEE Trans. Plasma Sci.*, vol. 48, no. 6, pp. 1512–1518, Jun. 2020, doi: 10.1109/TPS.2020.2963844.

[8] P. Luan, V. S. S. K. Kondeti, A. J. Knoll, P. J. Bruggeman, and G. S. Oehrlein, "Effect of water vapor on plasma processing at atmospheric pressure: Polymer etching and surface modification by an Ar/H2O plasma jet," *J. Vac. Sci. Technol. A*, vol. 37, no. 3, 2019, Art. no. 31305, doi: 10.1116/1.5092272.

[9] M. Narimisa, Y. Onyshchenko, R. Morent, and N. De Geyter, "Improvement of PET surface modification using an atmospheric pressure plasma jet with different shielding gases," *Polymer*, vol. 215, Feb. 2021, Art. no. 123421, doi: 10.1016/j.polymer.2021.123421.

[10] V. Jain, K. Nigam, N. Tanwani, S. Adam, S. Nimish, and S. K. Nema, "Novel high voltage pulsing to generate uniform glow discharge air plasma for environment friendly inline treatment of textile," in *Proc. IEEE Int. Pulsed Power Conf.*, 2019, pp. 1–3, doi: 10.1109/PPPS34859.2019.9009622.

[11] S. Reuter, T. Von Woedtke, and K. D. Weltmann, "The kINPen—A review on physics and chemistry of the atmospheric pressure plasma jet and its applications," *J. Phys. D. Appl. Phys.*, vol. 51, no. 23, 2018, Art. no. 233001, doi: 10.1088/1361-6463/aab3ad.

[12] S. Arndt, A. Schmidt, S. Karrer, and T. von Woedtke, "Comparing two different plasma devices kINPen and Adtec SteriPlas regarding their molecular and cellular effects on wound healing," *Clin. Plasma Med.*, vol. 9, pp. 24–33, Mar. 2018, doi: 10.1016/j.cpme.2018.01.002.

[13] M. Hofmans et al., "Characterization of a kHz atmospheric pressure plasma jet: Comparison of discharge propagation parameters in experiments and simulations without target," *Plasma Sources Sci. Technol.*, vol. 29, no. 3, 2020, Art. no. 34003, doi: 10.1088/1361-6595/ab6d49.

[14] P. Lin, J. Zhang, T. Nguyen, V. M. Donnelly, and D. J. Economou, "Numerical simulation of an atmospheric pressure plasma jet with coaxial shielding gas," *J. Phys. D. Appl. Phys.*, vol. 54, no. 7, 2021, Art. no. 75205, doi: 10.1088/1361-6463/abc2f1.

[15] H. Xu et al., "Contrasting characteristics of gas-liquid reactive species induced by pulse-modulated RF and kHz sinusoidal plasma jets," *IEEE Trans. Plasma Sci.*, vol. 47, no. 2, pp. 1336–1344, Feb. 2019, doi: 10.1109/TPS.2019.2891117.

[16] M. J. Johnson, G. H. Brown, D. R. Boris, T. B. Petrova, and S. G. Walton, "Two atmospheric pressure plasma jets driven by phase-shifted voltages: A method to control plasma properties at the plasma-surface interface," *IEEE Trans. Plasma Sci.*, vol. 50, no. 9, pp. 2961–2971, Sep. 2022, doi: 10.1109/TPS.2022.3198826.

[17] J. F. Kolb et al., "Cold atmospheric pressure air plasma jet for medical applications," *Appl. Phys. Lett.*, vol. 92, no. 24, 2008, Art. no. 241501, doi: 10.1063/1.2940325.

[18] P. Thana et al., "A compact pulse-modulation cold air plasma jet for the inactivation of chronic wound bacteria: Development and characterization," *Heliyon*, vol. 5, no. 9, 2019, Art. no. e02455, doi: 10.1016/j.heliyon.2019.e02455.

[19] E. J. Szili, S. H. Hong, J. S. Oh, N. Gaur, and R. D. Short, "Tracking the penetration of plasma reactive species in tissue models," *Trends Biotechnol.*, vol. 36, no. 6, pp. 594–602, 2018, doi: 10.1016/j.tibtech.2017.07.012.

[20] X. Lu, M. Keidar, M. Laroussi, E. Choi, E. J. Szili, and K. Ostrikov, "Transcutaneous plasma stress: From soft-matter models to living tissues," *Mater. Sci. Eng. R Rep.*, vol. 138, pp. 36–59, Oct. 2019, doi: 10.1016/j.mser.2019.04.002.

[21] B. Ghimire et al., "The role of UV photolysis and molecular transport in the generation of reactive species in a tissue model with a cold atmospheric pressure plasma jet," *Appl. Phys. Lett.*, vol. 114, no. 9, 2019, Art. no. 93701, doi: 10.1063/1.5086522.

[22] P. J. Bruggeman, N. Sadeghi, D. C. Schram, and V. Linss, "Gas temperature determination from rotational lines in non-equilibrium plasmas: A review," *Plasma Sources Sci. Technol.*, vol. 23, no. 2, 2014, Art. no. 23001, doi: 10.1088/0963-0252/23/2/023001.

[23] C. Schopp, N. Britun, J. Vorac, P. Synek, R. Snyders, and H. Heuermann, "Thermal and optical study on the frequency dependence of an atmospheric microwave argon plasma jet," *IEEE Trans. Plasma Sci.*, vol. 47, no. 7, pp. 3176–3181, Jul. 2019, doi: 10.1109/TPS.2019.2919245.

[24] S. Kelly and M. M. Turner, "Generation of reactive species by an atmospheric pressure plasma jet," *Plasma Sources Sci. Technol.*, vol. 23, no. 6, 2014, Art. no. 65013, doi: 10.1088/0963-0252/23/6/065013.

[25] D. Mance, R. Wiese, T. Kewitz, and H. Kersten, "Atmospheric pressure plasma jet for biomedical applications characterised by passive thermal probe," *Eur. Phys. J. D*, vol. 72, no. 6, p. 98, 2018, doi: 10.1140/epjd/e2018-80768-8.

[26] S. Hashimoto et al., "Understanding the role of plasma bullet currents in heating skin to mitigate risks of thermal damage caused by low-temperature atmospheric-pressure plasma jets," *Plasma*, vol. 6, no. 1, pp. 103–114, 2023, doi: 10.3390/plasma6010009.

[27] S. Kos, T. Blagus, M. Cemazar, G. Filipic, G. Sersa, and U. Cvelbar, "Safety aspects of atmospheric pressure helium plasma jet operation on skin: In vivo study on mouse skin," *PLoS One*, vol. 12, no. 4, pp. 1–15, 2017, doi: 10.1371/journal.pone.0174966.

[28] M. Witman, D. Gidon, D. B. Graves, B. Smit, and A. Mesbah, "Sim-to-real transfer reinforcement learning for control of thermal effects of an atmospheric pressure plasma jet," *Plasma Sources Sci. Technol.*, vol. 28, no. 9, 2019, Art. no. 95019, doi: 10.1088/1361-6595/ab3c15.

[29] D. Gidon, B. Curtis, J. A. Paulson, D. B. Graves, and A. Mesbah, "Model-based feedback control of a kHz-excited atmospheric pressure plasma jet," *IEEE Trans. Radiat. Plasma Med. Sci.*, vol. 2, no. 2, pp. 129–137, Mar. 2018, doi: 10.1109/TRPMS.2017.2764629.

[30] A. Mesbah and D. B. Graves, "Machine learning for modeling, diagnostics, and control of non-equilibrium plasmas," *J. Phys. D. Appl. Phys.*, vol. 52, no. 30, 2019, Art. no. 30LT02, doi: 10.1088/1361-6463/ab1f3f.

[31] D. Gidon, X. Pei, A. D. Bonzanini, D. B. Graves, and A. Mesbah, "Machine learning for real-time diagnostics of cold atmospheric plasma sources," *IEEE Trans. Radiat. Plasma Med. Sci.*, vol. 3, no. 5, pp. 597–605, Sep. 2019, doi: 10.1109/TRPMS.2019.2910220.